Single-molecule imaging reveals the roles of the membrane-binding motif and the C-terminal domain of RNase E in its localization and diffusion in *Escherichia coli*

Laura Troyer[1,6], Yu-Huan Wang[1,6], Shobhna[2,3], Seunghyeon Kim[1], Brooke Ramsey[4], Jeechul Woo[5], Emad Tajkhorshid[2,3,4*], and Sangjin Kim[1,4*]

[1]Department of Physics, University of Illinois Urbana-Champaign, Urbana, IL, USA
[2]Theoretical and Computational Biophysics Group, NIH Center for Macromolecular Modeling and Visualization, Beckman Institute for Advanced Science and Technology, University of Illinois Urbana-Champaign, Urbana, IL, USA
[3]Department of Biochemistry, University of Illinois Urbana-Champaign, Urbana, IL, USA
[4]Center for Biophysics and Quantitative Biology, University of Illinois Urbana–Champaign, Urbana, IL, USA
[5]Moduli Technologies, LLC, Springfield, IL, USA
[6]These authors contributed equally.
*Correspondence: emad@illinois.edu, sangjin@illinois.edu

ABSTRACT

In *Escherichia coli*, RNase E, a central enzyme in RNA processing and mRNA degradation, contains a catalytic N-terminal domain (NTD), a membrane-targeting sequence (MTS), and a C-terminal domain (CTD). We investigated how MTS and CTD influence RNase E localization, diffusion, and function. Super-resolution microscopy revealed that ~93% of RNase E localizes to the inner membrane and exhibits slow diffusion similar to polysomes. Comparing the native amphipathic MTS with a transmembrane motif showed that the MTS confers slower diffusion and stronger membrane binding. The CTD further slows diffusion by increasing mass but unexpectedly weakens membrane association. RNase E mutants with partial cytoplasmic localization displayed enhanced co-transcriptional degradation of *lacZ* mRNA. These findings indicate that variations in the MTS and the presence of the CTD shape the spatiotemporal organization of RNA processing in bacterial cells, providing mechanistic insight into how RNase E domain architecture influences its cellular function.

INTRODUCTION

RNase E (RNE) is the main endoribonuclease in *Escherichia coli*, known for its role in RNA processing and mRNA degradation[1-3]. It is an essential protein[4,5], and homologous proteins are found across many bacterial species[6-8]. The essentiality stems from the N-terminal domain (NTD), or the catalytic domain[9]. The NTD is followed by a membrane targeting sequence (MTS) and the C-terminal domain (CTD), or macromolecular interaction domain[2], where RhlB (a DEAD-box RNA helicase), PNPase (a 3'→5' exonuclease), and enolase (a glycolytic enzyme) bind to form the RNA degradosome complex[6]. The MTS forms an amphipathic α helix, responsible for the localization of RNE on the inner membrane[10,11]. Interestingly, the membrane localization of RNE and the presence of the CTD are not essential in *E. coli* nor are they conserved across bacterial species, in contrast to the broad conservation of the NTD across bacteria as well as chloroplasts[7,12,13]. This raises a question about the roles of membrane localization and the CTD in the *in vivo* function of RNE.

E. coli strains with cytoplasmic RNE (due to the removal of the MTS) are viable, although they grow more slowly than the wild-type (WT) cells[10,14]. *In vitro* studies have shown that membrane binding of RNE does not necessarily increase its enzymatic activity[10,14]. However, membrane localization is likely important for gene regulation *in vivo* because RNE becomes sequestered from the cytoplasmic pool of mRNAs, giving mRNAs time for translation. This idea is supported by our recent observation that the membrane-bound RNE limits the degradation of nascent mRNAs while cytoplasmic RNE (ΔMTS) can degrade nascent mRNAs during transcription[15]. We found that transcripts encoding membrane proteins can be an exception to this rule, in that they can experience co-transcriptional degradation assisted by the transertion effect[15]. These findings agree with results from a genome-wide study, indicating that the membrane localization of RNE allows for differential regulation of mRNA stability for genes encoding cytoplasmic proteins versus inner membrane proteins in *E. coli*[16].

Previous studies have reported evidence that *E. coli* RNE can localize in the cytoplasm—for example, when cells were grown anaerobically[17] or when membrane fluidity was reduced by changes in lipid composition[18]. These findings imply that RNE can

dissociate from the membrane; however, the origin of its weak membrane binding remains unknown.

Across bacteria, several species within α-proteobacteria have cytoplasmic RNE[19] while other species possess membrane-bound RNE. Among these, *B. subtilis* RNase Y (a functional homolog of RNE) associates with the membrane via a transmembrane (TM) motif[20], instead of an amphipathic motif used by *E. coli* and other γ-proteobacteria[7]. Given the diversity of membrane-binding motifs that have arisen through evolution, it should be possible to engineer *E. coli* RNE with a TM motif. Such a mutant would provide a useful model for investigating the impact of membrane-binding motifs on the localization, diffusion, and activity of RNE.

Lastly, the CTD of *E. coli* RNE is an intrinsically disordered region[21] that, while nonessential for cell viability, enhances the enzymatic activity of the NTD[15,22-24]. As the primary binding site for degradosome components[6], the CTD is thought to facilitate mRNA degradation by recruiting these proteins near the catalytic NTD. However, our recent study showed that these associated proteins have minimal impact on the degradation rate of *lacZ* mRNA, whereas deletion of the CTD markedly stabilizes the transcript[15], suggesting a possible intramolecular allosteric effect within RNE. In the present study, we further show that the CTD modulates the membrane binding affinity of RNE, possibly by affecting its conformation. These results reveal a previously underappreciated role of the CTD in regulating RNE function beyond degradosome assembly, with implications for how the spatial organization and structural dynamics of RNE fine-tune RNA degradation in bacteria.

In this study, we quantified the membrane binding percentage (MB%) of RNE in *E. coli* using single-molecule microscopy and showed that membrane association governs its diffusion and mRNA-degradation activity. Perturbing the native MTS, substituting it with LacY TM segments, and deleting the CTD collectively revealed how the MTS and CTD set RNE's spatial organization and provided routes for tuning activity through subcellular control.

RESULTS

Membrane binding percentage (MB%) of RNE

First, we investigated the subcellular localization of RNE in live cells. Previous fluorescence microscopy studies have shown that RNE is localized to the inner membrane in *E. coli*[10,11,16], but the percentage of membrane-bound molecules has not been quantitatively examined in live cells. To address this gap, we fused RNE with a photo-convertible fluorescent protein, mEos3.2[25] and imaged individual RNE molecules over time in two dimensions (**Fig. 1A**). The positions of fluorescent molecules were identified in each frame and linked into trajectories using the open-source software u-track[26] (**Fig. 1A**). In this section, we analyze localization, and diffusion dynamics are addressed in subsequent sections.

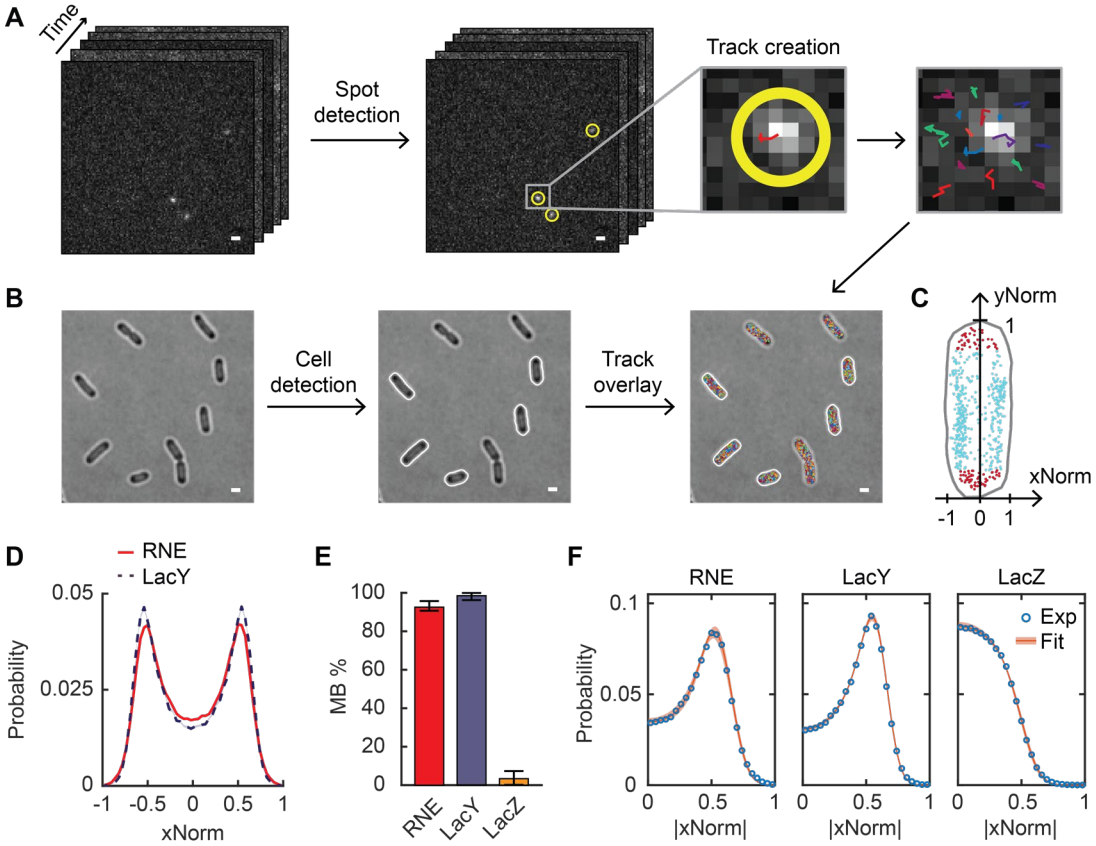

Figure 1: Analysis of single-molecule images for the subcellular localization and dynamics of proteins. (**A**) Single-molecule image analysis. Spots were detected in each frame (highlighted with yellow circles), and tracks were created across frames (different colors were chosen for different tracks). (**B**) Cell detection. Cell outlines were determined from bright-field images. Only non-dividing cells were analyzed (indicated by white outlines). (**C**) Normalized position of spots of RNE along the short (x) and the long (y) axes of an example cell. Red spots are inside the cell endcaps, and cyan spots are in the cylindrical region of the cell. (**D**) xNorm histogram of RNE and LacY. Only

spots in the cylindrical region of cells (like cyan spots in **C**) were included, totaling n = 143,000 spots. The standard error of the mean (SEM) calculated from bootstrapping is displayed as a shaded area but is smaller than the line width (see **Fig. S1A** for details). (**E**) The membrane binding percentage (MB%) of RNE, LacY, and LacZ. Error bars are from the 95% confidence interval. (**F**) Histogram of absolute xNorm and model fitting of RNE, LacY, and LacZ to determine MB%. Orange highlights indicate the range of xNorm expected based on the standard deviations in the parameter values estimated by MCMC. The white scale bars in panels **A**-**B** are 1 μm. See **Table S6** for data statistics.

Subcellular locations were calculated relative to the cell boundaries identified from bright-field images using another open-source image analysis package Oufti[27] (**Fig 1B**). To combine data from many cells, molecular positions along the short and long axes of a cell were normalized to the cell width and cell length, yielding xNorm and yNorm, respectively (**Fig. 1C**). Based on yNorm, molecules within the cylindrical part of the cell were selected, and their xNorm values were used to generate an xNorm histogram. Hereinafter, we focus on the xNorm histogram to compare the membrane enrichment across protein constructs.

The xNorm histogram of RNE shows two peaks corresponding to the inner membrane on each side of the cell (**Fig. 1D**, **Fig. S1A**), very similar to the xNorm histogram of LacY, obtained by imaging LacY-mEos3.2 using the same method. LacY is a membrane channel for lactose and is composed of 12 TM segments[28]. It is expected to be inserted into the inner membrane during translation[29-31], such that all imaged LacY is expected to be localized in the inner membrane[32].

We further quantified the percentage of molecules bound to the membrane (membrane-binding percentage or MB%) from the xNorm histogram. For this analysis, we first confirmed that proteins localized on the membrane and in the cytoplasm are detected with equal probability, despite differences in their mobilities (**Fig. S1B**-**C**). Next, we developed a mathematical model based on a 2D projection of molecules randomly distributed either on the surface of or within a cylinder. The model includes imaging effects that affect the shape of xNorm histograms: localization error, the limited focal depth of the quasi-TIRF illumination we used, and the location of the inner membrane relative to the cell boundary (**Fig. S1D**-**G**). Model fitting was performed using a Markov-Chain Monte

133 Carlo algorithm (MCMC). For validation, we applied the model to xNorm histograms of
134 LacY and LacZ, which serve as benchmarks for complete membrane binding and
135 complete cytoplasmic localization, respectively. The MB% of LacY was 99% with a 95%
136 confidence interval of [96%, 100%], and LacZ showed MB% of 3.4% [0.2%, 7.3%] (**Fig.**
137 **1E-F**). Both MB% agree with the expectations for membrane and cytoplasmic proteins.
138 For RNE, we found an MB% of 93% [91%, 96%] (**Fig. 1E**). The xNorm histogram of the
139 fastest 7% of the RNE population (based on the diffusion coefficient, as discussed below)
140 exhibited a cytoplasmic localization pattern (without the two membrane-associated
141 peaks), supporting the existence of a cytoplasmic RNE subpopulation (**Fig. S2A**).

142 We confirmed that the MTS (residue 568-582) is essential for the membrane binding
143 of RNE, as deletion of the MTS sequence made the xNorm like that of LacZ (**Fig. 2A-B**,
144 **Fig. S2D**). We note that the xNorm profile of RNE ΔMTS was slightly different from that
145 of LacZ near the center line of the cell (x = 0), suggesting fewer RNE ΔMTS molecules
146 were at the midline of the cell. Also, xNorm fitting yielded an MB% of 33%. These results
147 may reflect nucleoid exclusion of RNE ΔMTS due to its large size[33]. Consistently, a
148 smaller cytoplasmic RNE variant generated by CTD truncation (RNE (1-529) or RNE
149 ΔMTS ΔCTD) exhibited a xNorm profile closer to that of LacZ (**Fig. 2B**, **Fig. S2E**).

150 Is there a critical residue(s) within the MTS required for membrane binding? The MTS
151 forms an amphipathic α-helix, in which hydrophobic residues are expected to align on one
152 side of the helix (**Fig. 2C**)[10]. Previous studies suggested that replacing one of the
153 hydrophobic residues with a hydrophilic amino acid can disrupt membrane binding of
154 RNE[10,11]. We revisited the point mutations discussed in Khemici et al[10] and analyzed
155 MB% by mEos3.2 imaging. We found that the F574A F575A double mutation (noted as
156 F574AA) did not significantly affect MB%, consistent with the fact that the substituted
157 amino acids remain hydrophobic (**Fig. 2D-E**, **Fig. S2F**). In contrast, F582E and F575E
158 mutations reduced MB% to 47% and 50%, respectively (**Fig. 2E**), and their xNorm
159 histograms resembled that of RNE ΔMTS, suggesting predominantly cytoplasmic
160 localization (**Fig. 2D**, **Fig. S2D**, **S2G-H**). These findings indicate that the phenylalanine
161 residues at positions 575 and 582 are critical for membrane association of RNE.

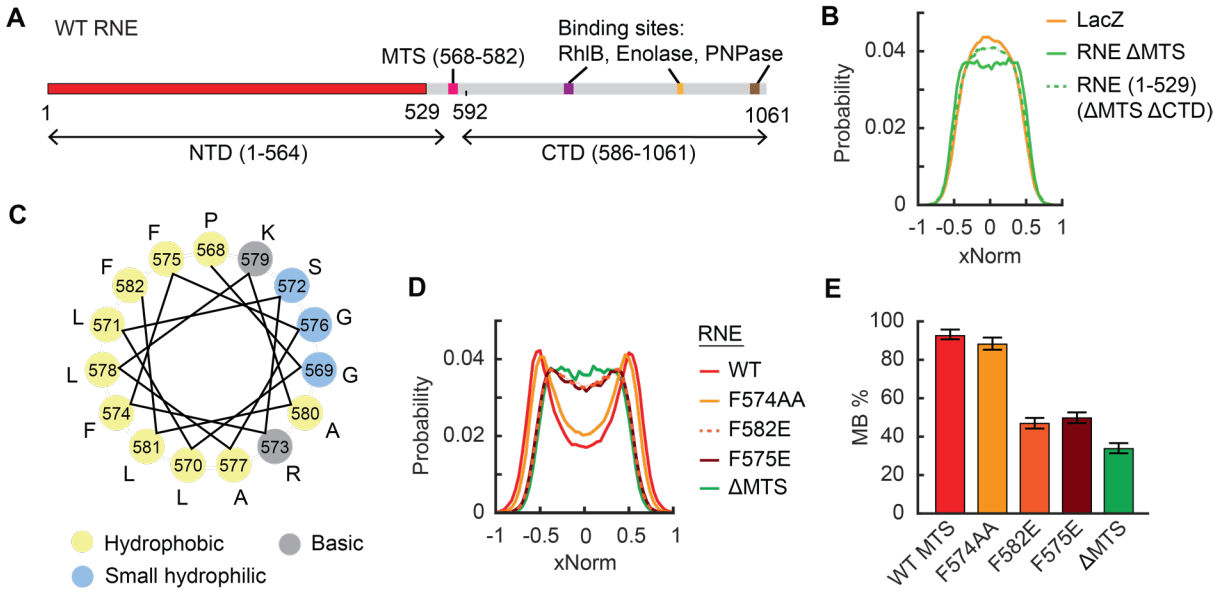

Figure 2: Mutations in the MTS affecting the localization of RNE. (**A**) Linear representation of the RNE monomer. The NTD and the CTD are defined as regions flanking the MTS. Numbers indicate the amino acid residues. (**B**) xNorm histograms of cytoplasmic RNE mutants. (**C**) Helical wheel diagram of the MTS region of RNE (residue 568-582). (**D**) xNorm histogram of RNE MTS point mutants. (**E**) MB% of RNE MTS point mutants. Error bars indicate the 95% confidence interval. In panels B and D, the SEM from bootstrapping is shown but is smaller than the line width. See **Table S6** for data statistics.

Effect of membrane binding on the diffusion of RNE

The membrane localization of RNE likely limits its diffusion and interaction with mRNA targets. Additionally, interaction with ribosome-bound mRNAs can further slow the diffusion of RNE. Here, we examined how these factors contribute to the diffusion dynamics of RNE.

To measure the diffusion of RNE, we analyzed the trajectories of individual RNE-mEos3.2 imaged at a 21.7-ms acquisition interval (**Fig. 1A**). We calculated the diffusion coefficient D by fitting the mean-squared displacement (MSD) of each trajectory to the equation MSD = $4D\tau + b$, where τ is lag time and b accounts for both dynamic and static localization errors[34] (**Fig. 3A**). We obtained D_{RNE} = 0.0184 ± 0.0002 μm²/s (mean ± SEM). This value was well above the lower detection limit of our microscope, determined using

174 stationary, surface-immobilized mEos3.2, D = 0.0020 ± 0.0001 μm^2/s (**Fig. S3A,**
175 **Supplementary Discussion**). Notably, D_{RNE} was comparable to that of ribosome-bound
176 mRNAs, estimated to be D ~0.015 μm^2/s based on the diffusion of ribosomal protein L1
177 (**Fig. S3B**).

178 To assess how membrane association affects diffusion, we compared D of WT RNE
179 and the ΔMTS mutant. These two proteins have similar molecular masses, as the MTS
180 comprises only 15 of the 1061 residues in a monomer of RNE (**Fig. 2A**). Therefore, any
181 difference in D can be attributed to their subcellular localizations (membrane vs
182 cytoplasm) rather than mass. We found that $D_{\Delta MTS}$ is ~5.5 times that of D_{RNE} (**Fig. 3B**).

183 We examined another pair of RNE mutants that differ in localization (membrane vs
184 cytoplasm) but are similar in size: membrane-bound RNE (1-592) and cytoplasmic RNE
185 (1-529), both lacking the CTD. These truncated variants diffused faster than their full-
186 length counterparts due to reduced mass, but their D values still differed by a factor of
187 ~5.3 due to localization (**Fig. 3B**). Together, these results suggest that the membrane
188 binding reduces RNE mobility by a factor of 5.

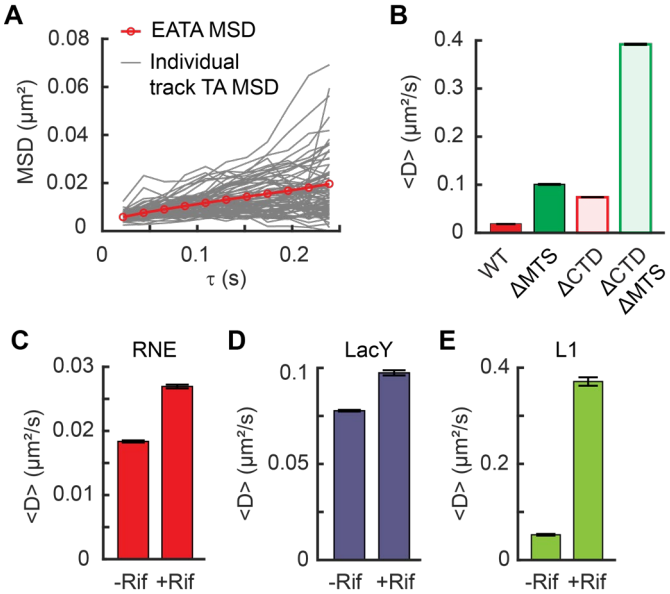

Figure 3: RNE diffusion, influenced by membrane binding and interactions with mRNAs. (**A**) MSD versus time delay (τ) for RNE. Ensemble-averaged time-averaged (EATA) MSD was calculated by averaging the time-averaged MSD of individual tracks. (**B**) Mean diffusion coefficients of various RNE mutants, lacking the MTS and/or the CTD. (**C-E**) Change in the mean diffusion coefficient of RNE (**C**), LacY (**D**), and

ribosome L1 protein (**E**) when cellular RNAs were depleted by rifampicin treatment. Error bars in panels B-E represent the SEM. See **Table S6** for data statistics.

189

190 **Diffusion of RNE in the absence of mRNA substrates**

191 When some of RNE molecules interact with mRNA, their diffusion can slow due to the
192 added mass of mRNA and ribosomes, possibly yielding slower RNE subpopulations.
193 Such mobility-based subpopulations have been observed for RNA polymerases and
194 ribosomes in *E. coli* and used to estimate the fraction of molecules interacting with RNA[35-
195 37].

196 To test the effect of mRNA substrates on RNE diffusion, we treated cells with
197 rifampicin (rif), which blocks transcription initiation, thus depleting cellular mRNAs[38]. In rif-
198 treated cells, D_{RNE} increased to 0.0270 ± 0.0003 μm^2/s, which is 1.47 ± 0.010 times that
199 in untreated cells (**Fig. 3C**). We note that D_{LacY} also increased to 1.25 ± 0.01 times relative
200 to untreated cells (**Fig. 3D**). Although this increase is relatively small, the increase in D_{LacY}
201 was unexpected because LacY is not an RNA-binding protein. The increase in D_{LacY} likely
202 results from the depletion of mRNAs near the membrane (e.g., the mRNAs undergoing
203 transertion), which could otherwise hinder the diffusion of membrane proteins[39,40]. The
204 similar fold change in D_{RNE} and D_{LacY} upon rif treatment suggests that the change in RNE
205 diffusion may largely be attributed to physical changes in the intracellular environment
206 (such as reduced viscosity or macromolecular crowding[41,42]), rather than a loss of RNA-
207 RNE interactions.

208 Because the rif-induced change in D_{RNE} is largely physical, we next examined why
209 eliminating RNA-RNE interactions does not further increase RNE mobility, using the
210 ribosome as a benchmark. The diffusion of ribosomal protein L1 became 7 times as fast
211 as that in rif-treated cells (**Fig. 3E**), consistent with previous reports[35,36]. This big change
212 can be explained by the fact that ribosomes form polysomes, where the effective mass of
213 L1 protein in untreated cells would be 2 or more times that in rif-treated cells (where it
214 remains as a free subunit). In the case of RNE, it forms the RNA degradosome complex,
215 whose mass can be from 450 kDa[6] to 2.3 MDa depending on the occupancy of the RNA
216 degradosome component proteins (RhlB, PNPase, enolase)[2,43-46] (**Supplementary**
217 **Discussion)**. Even at its largest size, the RNE complex is smaller than a 70S ribosome
218 (~2.5 MDa[47]). This means that if RNE interacts with an mRNA associated with n

219 ribosomes, the total mass of the RNE complex would increase by a factor of n or more.
220 Thus, a substantial increase in D_{RNE} would be expected upon mRNA depletion, assuming
221 that a significant fraction of RNE is engaged with mRNA-ribosome assemblies.

222 To explain the marginal increase in D_{RNE} upon rif treatment, we considered two
223 possibilities; (1) only a small percentage of RNE molecules interacts with mRNAs at a
224 given time and/or (2) RNE interacts with mRNAs only briefly, unlike ribosomes which
225 spend an order of 10-100 s in a polysome state during translation elongation[48]. To
226 distinguish between these possibilities, we attempted to increase the cellular pool of
227 polysomes, either by treating cells with a translation elongation inhibitor
228 chloramphenicol[37] or by overexpressing *lacZ* mRNA from a high-copy plasmid (**Fig. S3D-**
229 **E**). In both cases, a larger fraction of RNE would engage with mRNAs, potentially
230 increasing the fraction of RNE in the slow-diffusing state. However, D_{RNE} remained
231 unchanged compared to untreated cells (**Fig. S3F**). This result rules out the possibility
232 that only a small percentage of RNE interacts with mRNAs and instead weighs in favor of
233 the scenario that RNE-mRNA interactions are brief. Specifically, if RNE interacts with
234 mRNAs for ~20 ms or less, the slow-diffusing state would last shorter than the frame
235 interval and remain undetected in our experiment.

236

237 **Diffusion and localization of the MTS and TM segments**

238 Unlike RNE in *E. coli*, RNase Y, a functional homolog of RNE in *B. subtilis*, is localized to
239 the membrane via a TM domain[20]. We wondered if there are differences between a
240 peripheral motif (like the MTS of *E. coli*'s RNE) and a TM motif in terms of membrane
241 localization and mobility. To address this question, we created RNE mutants in which the
242 MTS was replaced with a TM domain. For the TM domain, we used TM segments of LacY,
243 a native *E. coli* protein, rather than using the TM motif from *B. subtilis* RNase Y, which
244 might interact with the *E. coli* membrane in a non-native manner.

245 Before creating the RNE mutants, we characterized the MB% and the diffusion of
246 individual short membrane-binding motifs. Native LacY contains 12 TM segments,
247 arranged into two groups of six[28]. We successfully expressed constructs containing the
248 first two TM segments (LacY (1-74) or LacY2), the first six TM segments (LacY (1-193)
249 or LacY6), and the full-length LacY (LacY12), each fused to mEos3.2 and expressed from

250 a chromosomal IPTG-inducible promoter (**Fig. 4A**). We then imaged their membrane
251 localization and diffusion. Both the MTS segment and LacY-derived TM segments
252 showed a strong membrane enrichment (**Fig. 4B**). In terms of diffusion, LacY2 and LacY6
253 diffused faster than the MTS segment (**Fig. 4C**), contrary to expectations based on size
254 (or mass)-dependent diffusion (**Fig. 4D**).

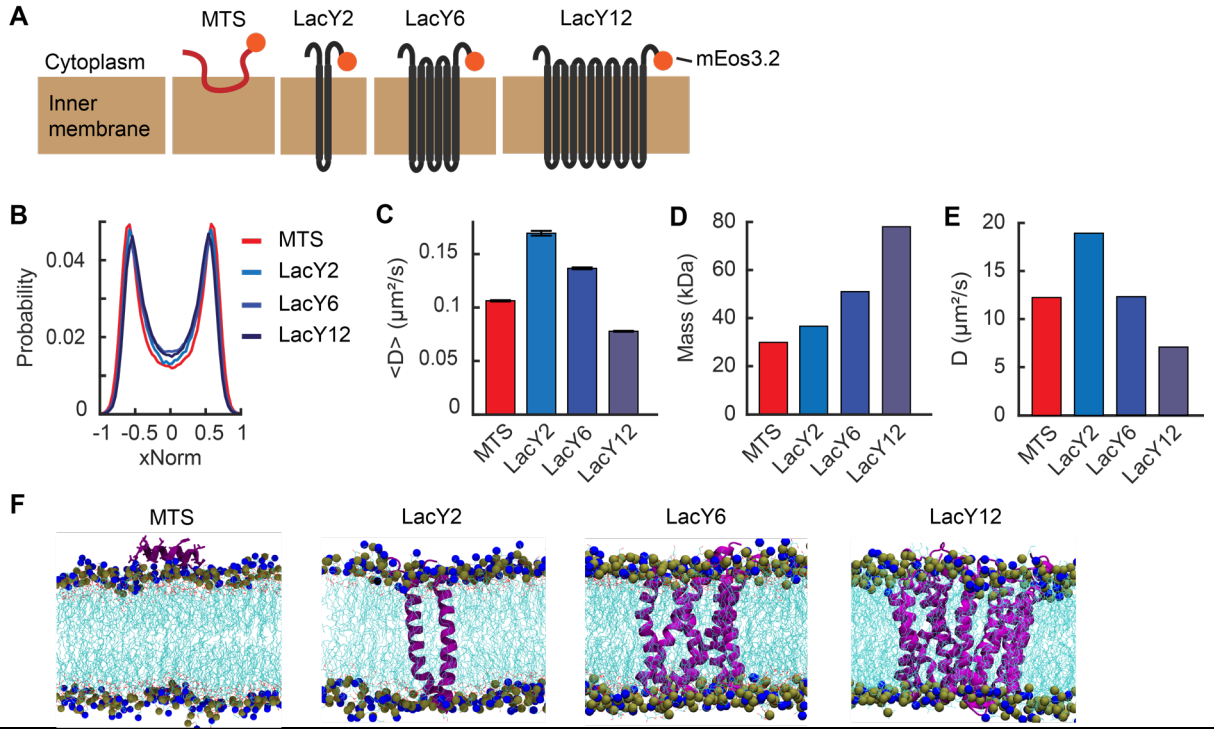

Figure 4: Localization and diffusion of membrane-binding motifs. (**A**) Cartoon schematic of the membrane-binding motifs used in this study (not to scale). The orange circles indicate mEos3.2 used for imaging. (**B**) xNorm histograms of membrane-binding motifs. The SEM from bootstrapping is displayed but smaller than the line width. Data are from at least 107,000 spots. (**C**) Mean diffusion coefficients of membrane-binding motifs. Error bars are the SEM from at least 3,000 tracks. (**D**) Estimated mass of membrane-binding motifs based on the amino acid sequence including linkers and mEos3.2. (**E**) Diffusion coefficients of the membrane-binding motifs obtained from all-atom MD simulation. (**F**) Representative simulation snapshots of the membrane-binding motifs embedded in the *E. coli* membrane. Proteins are displayed in purple, and lipid tails are shown in cyan. Nitrogen and phosphorus atoms of the lipid head groups are represented in the van der Waals form in blue and grey, respectively. See **Table S6** for data statistics.

255

256 According to the Stokes-Einstein relation for diffusion in simple fluids[49] and the
257 Saffman-Delbruck diffusion model for membrane proteins[50], *D* decreases as particle size

258 increases, albeit with different scaling behaviors. Specifically, the Saffman-Delbruck
259 model predicts that *D* for membrane proteins decreases logarithmically with increasing
260 radius of the membrane-embedded region, assuming a constant membrane
261 environment[50]. Thus, if size (or mass) were the primary determinant of diffusion, LacY2
262 and LacY6 would diffuse more slowly than the smaller MTS. The observed discrepancy
263 instead implies that *D* may be governed by how each motif interacts with the membrane.
264 For example, the way that TM domains are anchored to the membrane may facilitate
265 faster lateral diffusion with surrounding lipids.

266 Despite the prevalence of peripheral membrane proteins[51], how they interact with the
267 membrane and how this differs from TM proteins remain poorly understood. To further
268 explore this, we conducted all-atom molecular dynamics (MD) simulations of the MTS and
269 the LacY variants interacting with the *E. coli* membrane using the NAMD software[52]. In
270 the simulations, protein motion was calculated for 1 μs. Although the absolute *D* values
271 were higher than experimental values (possibly due to the absence of mEos3.2 in the
272 model), the overall trends were preserved; among the LacY series, larger constructs
273 diffused more slowly (**Fig. 4E**-**F**, **Fig. S4A**). Most importantly, the MTS again diffused
274 more slowly than LacY2 *in silico* (**Fig. 4E**, **Fig. S4A**). By calculating membrane-protein
275 interaction energies, we found that the MTS-membrane interactions were more stable
276 than those of LacY2 (**Fig. S4B**). These results suggest that the slower diffusion of the
277 MTS is due to stronger interactions with lipid head groups compared to membrane-
278 embedded TM segments.

279

280 **RNE mutants carrying a TM motif**

281 Since LacY2 and LacY6 showed strong membrane enrichment similar to LacY12 (**Fig.**
282 **4B**), we replaced the MTS in RNE with LacY2, LacY6, and LacY12 in the presence or
283 absence of the CTD (**Fig. 5A**-**B** and **Fig. S5**). All chimeric RNE mutants were expressed
284 from the native chromosomal locus as the only copy of *rne*, with mEos3.2 fused at the C
285 terminus for imaging. The resulting strains exhibited no noticeable differences in growth
286 rate compared to the WT strain (**Table S3**), suggesting that the RNE mutants were
287 functionally active.

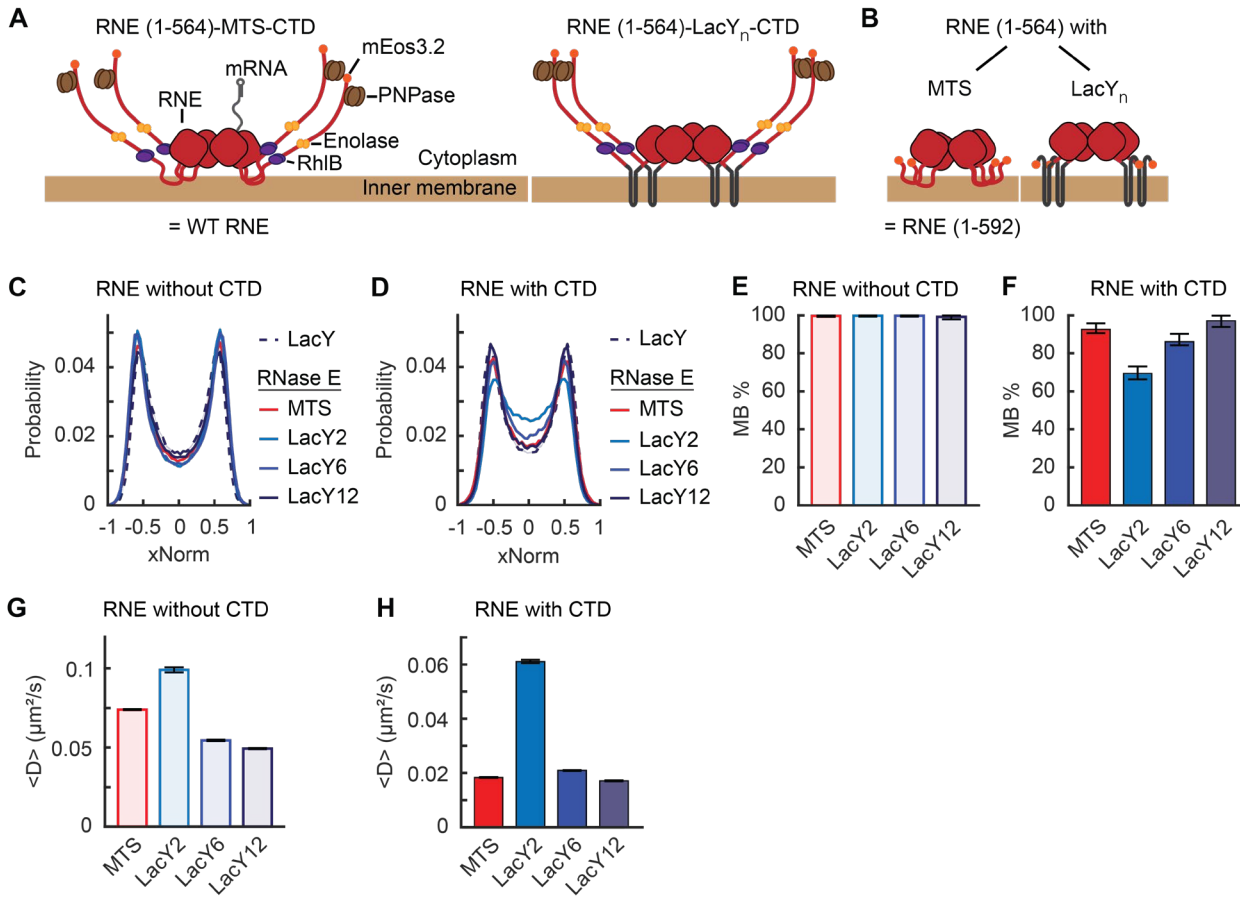

Figure 5: Localization and diffusion of chimeric RNE with or without the CTD. (**A-B**) Cartoon schematic of RNE chimeric variants with the CTD (**A**) and without the CTD (**B**). They are not to scale. (**C-D**) xNorm histograms of chimeric RNE localization compared with that of LacY. The SEM from bootstrapping is displayed but smaller than the line width. (**E-F**) MB% of chimeric RNE mutants without the CTD (**E**) or with the CTD (**F**) with various membrane-binding motifs. Error bars are from a 95% confidence interval. (**G-H**) Mean diffusion coefficients of chimeric RNE without the CTD (**G**) or with the CTD (**H**). Error bars are the SEM. Each data set contains at least 70,000 tracks for diffusion or 72,000 spots for xNorm. See **Table S6** for data statistics.

xNorm histograms of the ΔCTD mutants indicated membrane localization similar to LacY (**Fig. 5C**). However, mutants containing the CTD showed noticeable cytoplasmic subpopulations when LacY2 and LacY6 were used in place of the MTS (**Fig. 5D**, **Fig. S2J-K**, **Fig. S6B**). Mathematical model fitting of the xNorm histograms estimated the MB% of RNE-LacY2-CTD and RNE-LacY6-CTD to be 69% [66%, 73%] and 86% [84%, 90%], respectively (**Fig. 5F**). We note that imperfect membrane localization was observed

295 only in mutants containing the CTD; the same protein without the CTD showed MB% of
296 100% (**Fig. 5E-F, Fig. S6A-B**). These findings suggest that the CTD may contribute to
297 unstable membrane binding of RNE. Supporting this idea, previously characterized RNE
298 MTS point mutants with MB% <50% (**Fig. 2D-E**) also exhibited increased MB% upon the
299 CTD removal (**Fig. S6A-B**). Such a difference in MB% between the CTD-containing and
300 the CTD-lacking mutants was not observed in the chimera based on LacY12 (**Fig. 5E-F**),
301 possibly due to the stable membrane insertion by LacY12.

302 Next, we examined whether the *D* of chimeric RNE mutants varied depending on the
303 type of membrane-binding motifs. For example, the MTS diffused more slowly than LacY2
304 and LacY6, despite being smaller in size (**Fig. 4C-D**). Based on this, we expected the
305 chimeric RNE with LacY2 or LacY6 to diffuse faster than RNE with MTS. Indeed, in the
306 absence of the CTD, we found that the *D* of LacY2-based RNE was 1.33 ± 0.01 times as
307 fast as the MTS-based RNE (**Fig. 5G**). However, LacY6-based RNE did not diffuse faster
308 than the MTS-based version (**Fig. 5G**). This result may be due to the high TM load (24
309 helices) created by four LacY6 anchors in the RNE tetramer. Although all constructs are
310 tetrameric, the 24-helix load (LacY6), compared with 8 (LacY2) and 4 (MTS), likely
311 enlarges the membrane-embedded footprint and increases drag, thereby changing the
312 mobility advantages assessed as standalone membrane anchors.

313 In the presence of the CTD, the *D* of LacY2 and LacY6-based RNE became 3.33 ±
314 0.004 and 1.14 ± 0.01 times that of the MTS-based RNE counterpart (i.e. the WT RNE),
315 respectively (**Fig. 5H**). This is likely influenced by the presence of a cytoplasmic
316 population (~31% for LacY2 and ~14% for LacY6; **Fig. 5F**, **Fig S2J-K**), which diffuses
317 more rapidly than membrane-bound molecules (possibly by a factor of five, based on **Fig.**
318 **3B**). Taken together, our data suggest that the CTD weakens the membrane association
319 of RNE and small TM motifs can facilitate the diffusion of RNE.

320

321 **Functional consequence of subcellular localization and diffusion of RNE**

322 To check the functional consequence of cytoplasmic localization of RNE, we measured
323 *lacZ* mRNA degradation in various RNE mutants presented in this study. Recently, we
324 developed an assay to quantify both co-transcriptional and post-transcriptional
325 degradation rates of *lacZ* mRNA by inducing its transcription for only 75 s, thereby

326 capturing the degradation of nascent mRNA[15]. In WT cells, we found that the co-
327 transcriptional degradation rate (k_{d1}) is about 10 times slower than the post-transcriptional
328 degradation rate (k_{d2})[15]. In cells expressing RNE ΔMTS, however, k_{d1} increases by a factor
329 of ~3, suggesting that cytoplasmic RNE can freely diffuse and degrade nascent mRNAs[15].
330 This result led us to hypothesize that RNE variants exhibiting a cytoplasmic subpopulation
331 (**Fig. 2E** and **5F**) may exhibit a larger k_{d1} compared to more membrane-bound variants.

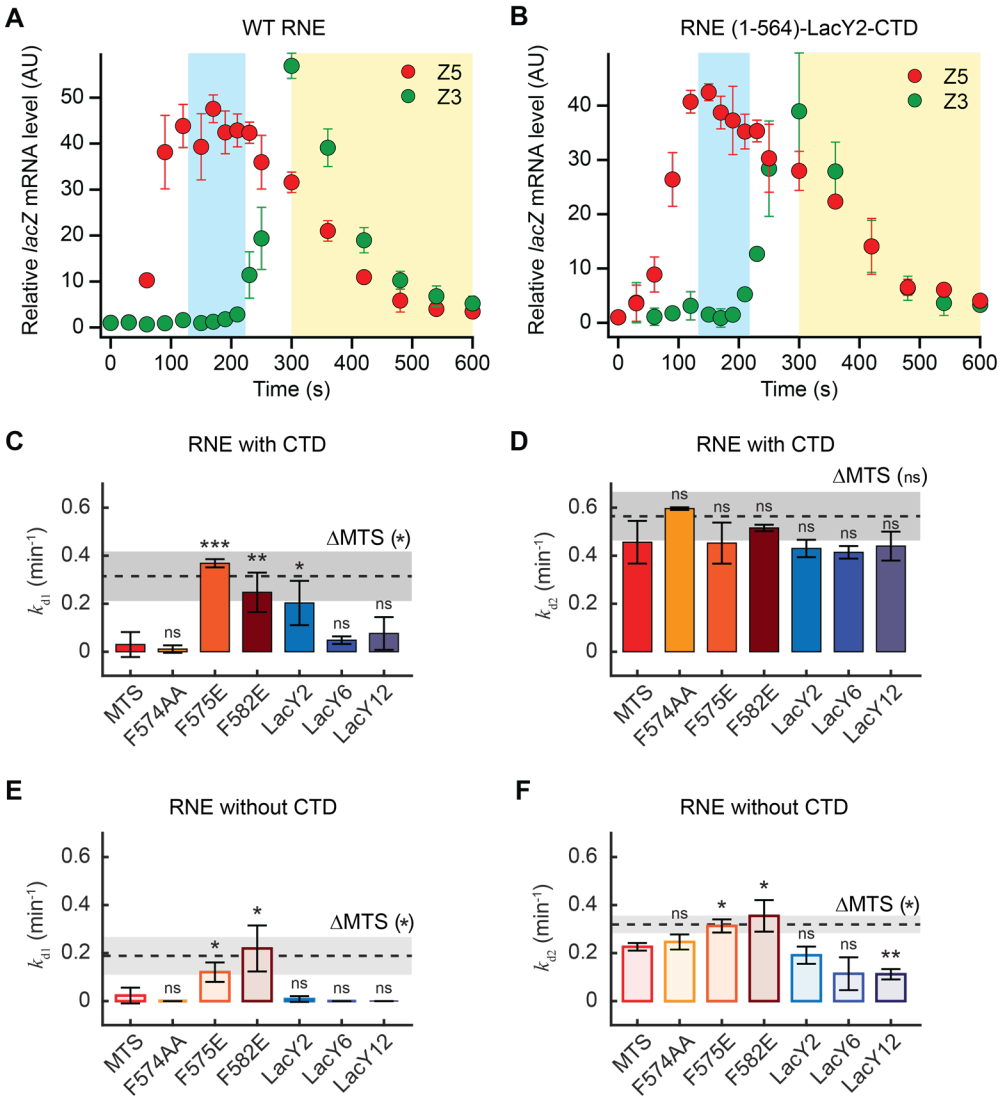

Figure 6: *lacZ* mRNA degradation rates in RNE mutant strains. (**A-B**) *lacZ* mRNA levels in WT RNE (**A**, strain SK595) and in RNE-LacY2-CTD (**B**, strain SK505) when *lacZ* transcription was induced with 0.2 mM IPTG at t = 0 s and re-repressed with 500 mM glucose at t = 75 s. Blue and yellow regions indicate the time windows used to measure k_{d1} and k_{d2}, respectively, by exponential fitting of 5' *lacZ* mRNA (Z5) in individual

replicates. (**C-F**) Co-transcriptional and post-transcriptional *lacZ* mRNA degradation rates, k_{d1} (**C, E**) and k_{d2} (**D, F**), respectively, in various RNE mutants containing different membrane-binding motifs, either with the CTD (solid bars, **C-D**) or ΔCTD (light bars, **E-F**). The dotted lines indicate the k_{d1} and k_{d2} values of cytoplasmic RNE ΔMTS (strain SK339 in **C-D**)[15] or RNE ΔMTS ΔCTD (strain SK370, in **E-F**). In all panels, error bars represent the standard deviations from 2-3 biological replicates. Two-sample *t*-tests were performed relative to the MTS case in each graph (See **Table S7** for the *p* values).

We repeated this assay in a strain expressing the WT RNE fused to mEos3.2 (**Fig. S7A**). Note that this strain is different from the one we used for imaging because a monocistronic *lacZ* gene is needed for the transient induction assay[15]. The relative abundances of 5' *lacZ* mRNA (Z5) remained constant prior to the rise in 3' *lacZ* mRNA (Z3) levels (between ~100 and 210 s), confirming negligible co-transcriptional degradation in WT cells[15] (**Fig. 6A**). However, in cells expressing RNE-LacY2-CTD (MB% = 69%), Z5 levels exhibited a downward trend during the same time window (**Fig. 6B**). The estimated k_{d1} was close to what was observed in RNE ΔMTS[15] (gray line, p = 0.28; **Fig. 6C**). A similarly high k_{d1} was also observed in RNE MTS point mutations, F582E and F757E, which exhibited a ΔMTS-like xNorm profile (**Fig. 2D**), supporting the idea that the cytoplasmic subpopulation of RNE enables co-transcriptional mRNA degradation in *E. coli* (**Fig. 6C**). Notably, RNE-LacY6-CTD, which also exhibited a cytoplasmic subpopulation (~14% from MB% of 86%), did not exhibit a significant increase in k_{d1} (**Fig. 6C**), suggesting a critical amount of cytoplasmic population may be needed to facilitate co-transcriptional mRNA degradation

We next examined whether the post-transcriptional mRNA degradation rate (k_{d2}) is limited by the slow diffusion of membrane-bound RNE. In the presence of the CTD, k_{d2} did not significantly vary across membrane-targeting variants (**Fig. 6D**). For example, even though the LacY12 motif slows RNE diffusion, its k_{d2} was similar to that of WT RNE (**Fig. 6D**). A critical control for this comparison is RNE abundance: because RNE autoregulates its expression by degrading its own transcript[53], slower diffusion could elevate RNE levels and mask the negative effect of the reduced mobility. We tested this explicitly and found that over-expression of WT RNE does not significantly change k_{d1} or k_{d2} (**Fig. S7B**). Thus, when the CTD is present, neither copy number nor diffusion of membrane-bound RNE limits k_{d2}.

358 In the absence of the CTD, k_{d1} was high in RNE variant F582E (MB% = 67%; **Fig.**
359 **S6A**), reaching levels close to its cytoplasmic counterpart, the ΔMTS ΔCTD mutant (gray
360 line, p = 0.7; **Fig. 6E**). k_{d2} values for ΔCTD variants were, in general, lower than those of
361 their CTD-containing counterparts (**Fig. 6F**), indicating the importance of the CTD for the
362 catalytic activity. These findings are consistent with previous reports on RNE constructs
363 based on the MTS[15,22-24]. Among ΔCTD variants with different membrane motifs, point
364 mutants F575E and F582E (MB% = 91% and 67%, respectively; **Fig. S6A**) exhibited
365 higher k_{d2} than the MTS-based variant, in agreement with the fact that completely
366 cytoplasmic ΔMTS ΔCTD exhibited higher k_{d2} than the MTS-containing ΔCTD (**Fig. 6F**).
367 However, the LacY2-based RNE variant, which diffuses faster than the MTS version (**Fig.**
368 **5G**), did not show a corresponding increase in k_{d2} (**Fig. 6F**). Plus, LacY6 and LacY12
369 versions showed even lower k_{d2} than MTS-based RNE ΔCTD. Overall, these results
370 indicate that the reduced k_{d2} caused by ΔCTD cannot be rescued by faster diffusion of
371 membrane-bound RNE. In fact, it may be further impaired by large and slow membrane
372 motifs (such as LacY12). The presence of the CTD appears to buffer the effects of large
373 membrane-binding motifs on RNE's catalytic activity, helping to maintain efficient post-
374 transcriptional mRNA degradation (k_{d2}).
375
376 **DISCUSSION**
377 Our study establishes the membrane enrichment and slow diffusion of RNE in *E. coli*.
378 This supports the notion that sequestration of RNE on the membrane confers the spatial
379 and temporal separation between synthesis and decay of mRNAs[15]. Furthermore, the
380 processing of rRNA[54-58] and tRNA[59,60] and small RNA-based gene regulations[61,62]
381 mediated by RNE likely take place on the membrane.
382 For WT RNE, our analysis showed MB% of 93%, close to 91% previously reported
383 using immunogold labeling and freeze-fracture electron microscopy[63]. Whether the MB%
384 of RNE changes under different growth conditions remains to be tested. As a case study,
385 we examined the MB% of WT RNE when cells were grown in M9 minimal medium with
386 succinate as the sole carbon source without supplements, a condition different from that
387 used in our primary experiments (M9 glycerol with supplements). The MTS segment
388 exhibited a reduction in MB% from 100% to 83% (**Fig. S6C**), suggesting that MTS-

389 mediated membrane binding can be sensitive to growth conditions. However, the MB%
390 of WT RNE was only marginally affected by the same media change (**Fig. S6C**). We
391 speculate that tetramer formation stabilizes RNE membrane localization, even when
392 individual MTS motifs exhibit a weak membrane affinity. A similar phenomenon has been
393 observed with MinD; although its amphipathic motif alone is cytoplasmic, MinD becomes
394 membrane-associated upon dimerization, indicating that oligomerization enhances the
395 membrane binding of this peripheral membrane protein[64]. By analogy, the tetrameric
396 structure of RNE may reinforce membrane association, buffering against changes in
397 cellular metabolism or lipid environment that would otherwise weaken MTS-mediated
398 binding.

399 While individual TM motifs exhibited strong membrane association regardless of
400 growth conditions (**Fig. S6D**), we found LacY2-based RNE can lose membrane binding
401 affinity, unlike MTS-based RNE. The loss of MB% in LacY2-based RNE was observed
402 only in the presence of the CTD (**Fig. S6D**), suggesting that the CTD negatively affects
403 membrane binding of RNE, possibly by altering protein conformation. In fact, all ΔCTD
404 RNE mutants we tested exhibited higher MB% than their CTD-containing counterparts
405 (**Fig. S6A**-**B**). For example, WT RNE (containing CTD) showed an MB% of 93%, whereas
406 its ΔCTD version, RNE (1-592), showed 100%. Similarly, the chimeric RNE-LacY6-CTD
407 showed an MB% of 86%, while its ΔCTD version showed 100% (**Fig. 5E**-**F**, **Fig. S6A**-**B**).
408 A similar trend was observed for MTS point mutants (**Fig. S6A**-**B**), further supporting that
409 the CTD decreases membrane association across RNE variants. We speculate that this
410 effect may be related to the CTD's role in promoting phase-separated ribonucleoprotein
411 condensates, as observed in *Caulobacter crescentus*[19]. In *E. coli*, we also observed a
412 modest increase in the clustering tendency of RNE compared to ΔCTD (**Fig. S8**).

413 The D_{RNE} we measured in *E. coli* (0.018 $\mu m^2/s$) is comparable to those measured in
414 other bacterial species. For example, in *C. crescentus*, the *D* of its cytoplasmic RNE was
415 shown to be about 0.03 $\mu m^2/s$[65]. The diffusion of RNase Y in *B. subtilis* was found in either
416 a slow (0.031 $\mu m^2/s$) or fast (0.3 $\mu m^2/s$) population[66], with the slow population
417 corresponding to RNase Y bound to mRNA and/or the putative RNA degradosome and
418 the fast population representing freely diffusing RNase Y. In the case of *E. coli* RNE, a
419 two-population fit of the *D* histogram based on MB% identified the slow and fast

420 subpopulations whose *D* values differed by a factor of 4 (**Fig. S3C**). This agrees with our
421 finding that cytoplasmic RNE ΔMTS diffuses ~5 times as fast as WT RNE on average
422 (**Fig. 3B**).

423 Diffusion is affected by the size of the particle in a given medium[50], and it has been
424 used to identify different size forms of a protein due to biochemical interactions or complex
425 formation[36,67]. Related, RNA substrates interacting with RNE can also increase the
426 effective mass of RNE and lower its *D* value. However, when cellular mRNAs were
427 depleted by rifampicin treatment, RNE diffusion increased less than that of other RNA-
428 binding proteins related to transcription and translation. For example, the large and small
429 ribosomal subunits[35,36,68], tRNA[69], and RNA polymerase[37] showed a large (about 10-20
430 fold) increase in *D* upon rifampicin treatment. Interestingly, Hfq, an RNA chaperon
431 involved in small RNA regulation together with RNE, showed a moderate increase (~2
432 fold) in *D* when RNA was depleted by rifampicin[70]. We note that our result is consistent
433 with previous studies that examined the effect of rifampicin on RNE diffusion in *E. coli*[11,71]
434 as well as RNE in *C. crescentus*[65] and RNase Y in *B. subtilis*[66,72]. One possible
435 explanation is that RNA-bound RNE (and RNase Y) is short-lived compared to our frame
436 interval (~20 ms), unlike other RNA-binding proteins related to transcription and
437 translation, interacting with RNA for ~1 min for elongation[48].

438 Lastly, the slow diffusion of the MTS in comparison to LacY2 and LacY6 suggests that
439 MTS is less favorable for rapid lateral motion in the membrane. Our MD simulations
440 demonstrated that this reduced diffusivity may originate from a stronger interaction energy
441 between the protein and the membrane. Whether this property is specific to the MTS or
442 generalizable to other peripheral versus integral membrane motifs remains to be tested.
443 We speculate that this can be a general phenomenon, as peripheral motifs interact with
444 lipids orthogonally while integral membrane motifs align parallel to the bilayer and may
445 diffuse more freely by coupling with the motion of surrounding lipids. The diffusion
446 behavior of membrane-bound proteins reflects underlying protein-lipid interactions and
447 membrane dynamics[73]. Accordingly, future work may analyze how protein-lipid interaction
448 strength and membrane dynamics contribute to differences in lateral diffusion between
449 peripheral and integral membrane proteins.

450 Altogether, our work highlights strategies to modulate the MB% and diffusion of RNE
451 to possibly affect mRNA degradation rates. For example, membrane-bound RNE lacking
452 the CTD can stabilize mRNAs and increase protein expression. This idea has been used
453 in a commercial *E. coli* BL21 strain (Invitrogen's One Shot BL21 Star) to increase
454 recombinant protein yield[22]. Additionally, RNE variants with environmentally responsive
455 MB%, such as RNE-LacY2-CTD, could be harnessed to tune mRNA half-lives and protein
456 expression levels under different growth conditions.
457

458 **ACKNOWLEDGMENTS**

459 We thank Drs. Mark Arbing, Agamemnon Carpousis, Johan Elf, and Christine Jacobs-
460 Wagner for strains. We thank Maggie Liu, Kavya Vaidya, and Zach Wang for their
461 contributions in the early phase of this work and the members of Kim lab for critical
462 reading of the manuscript. This work was supported by the NSF Center for Physics of
463 Living Cells (1430124), NSF Science and Technology Center for Quantitative Cell Biology
464 (2243257), NIH (R35GM143203; R24GM145965), and Searle Scholars Program.
465

466 **AUTHOR CONTRIBUTIONS**

467 L.T. and S.K. designed the research; L.T. and Y.W. performed imaging and analysis; L.T.
468 and Se.K. measured mRNA lifetimes; LT, Se.K., and S.K. performed genetics; L.T., Y.W.,
469 and J.W. developed data analysis methods; S. performed all-atom MD simulations under
470 supervision of E.T.; B.R. performed epi-fluorescence imaging; L.T. and S.K. wrote the
471 manuscript with input from all authors; S.K. supervised the study.
472

473 **COMPETING INTERESTS**

474 The authors declare no competing interests.
475

476 **REFERENCES**

477 1 Mudd, E. A., Krisch, H. M. & Higgins, C. F. RNase E, an endoribonuclease, has a
478 general role in the chemical decay of Escherichia coli mRNA: evidence that rne
479 and ams are the same genetic locus. *Molecular Microbiology* **4**, 2127-2135
480 (1990). https://doi.org/https://doi.org/10.1111/j.1365-2958.1990.tb00574.x

481 2 Mackie, G. A. RNase E: at the interface of bacterial RNA processing and decay.
482 *Nature Reviews Microbiology* **11**, 45-57 (2013).
483 https://doi.org/10.1038/nrmicro2930
484 3 Hui, M. P., Foley, P. L. & Belasco, J. G. Messenger RNA degradation in bacterial
485 cells. *Annual Review of Genetics* **48**, 537-559 (2014).
486 https://doi.org/https://doi.org/10.1146/annurev-genet-120213-092340
487 4 Apirion, D. & Lassar, A. B. A conditional lethal mutant of Escherichia coli which
488 affects the processing of ribosomal RNA. *Journal of Biological Chemistry* **253**,
489 1738-1742 (1978). https://doi.org/https://doi.org/10.1016/S0021-9258(17)34927-
490 X
491 5 Babitzke, P. & Kushner, S. R. The Ams (altered mRNA stability) protein and
492 ribonuclease E are encoded by the same structural gene of Escherichia coli.
493 *Proceedings of the National Academy of Sciences* **88**, 1-5 (1991).
494 https://doi.org/doi:10.1073/pnas.88.1.1
495 6 Carpousis, A. J. The RNA degradosome of Escherichia coli: an mRNA-degrading
496 machine assembled on RNase E. *Annual Review of Microbiology* **61**, 71-87
497 (2007). https://doi.org/https://doi.org/10.1146/annurev.micro.61.080706.093440
498 7 Aït-Bara, S. & Carpousis, A. J. RNA degradosomes in bacteria and chloroplasts:
499 classification, distribution and evolution of RNase E homologs. *Molecular*
500 *Microbiology* **97**, 1021-1135 (2015).
501 https://doi.org/https://doi.org/10.1111/mmi.13095
502 8 Mardle, C. E. *et al.* A structural and biochemical comparison of ribonuclease E
503 homologues from pathogenic bacteria highlights species-specific properties.
504 *Scientific Reports* **9**, 7952 (2019). https://doi.org/10.1038/s41598-019-44385-y
505 9 Callaghan, A. J. *et al.* Structure of Escherichia coli RNase E catalytic domain and
506 implications for RNA turnover. *Nature* **437**, 1187-1191 (2005).
507 https://doi.org/10.1038/nature04084
508 10 Khemici, V., Poljak, L., Luisi, B. F. & Carpousis, A. J. The RNase E of
509 Escherichia coli is a membrane-binding protein. *Molecular Microbiology* **70**, 799-
510 813 (2008). https://doi.org/10.1111/j.1365-2958.2008.06454.x
511 11 Strahl, H. *et al.* Membrane recognition and dynamics of the RNA degradosome.
512 *PLOS Genetics* **11**, e1004961 (2015).
513 https://doi.org/10.1371/journal.pgen.1004961
514 12 Kaberdin, V. R. *et al.* The endoribonucleolytic N-terminal half of Escherichia coli
515 RNase E is evolutionarily conserved in Synechocystis sp. and other bacteria but
516 not the C-terminal half, which is sufficient for degradosome assembly.
517 *Proceedings of the National Academy of Sciences* **95**, 11637-11642 (1998).
518 https://doi.org/doi:10.1073/pnas.95.20.11637
519 13 Lee, K. & Cohen, S. N. A Streptomyces coelicolor functional orthologue of
520 Escherichia coli RNase E shows shuffling of catalytic and PNPase-binding
521 domains. *Molecular Microbiology* **48**, 349-360 (2003).
522 https://doi.org/https://doi.org/10.1046/j.1365-2958.2003.03435.x
523 14 Hadjeras, L. *et al.* Detachment of the RNA degradosome from the inner
524 membrane of Escherichia coli results in a global slowdown of mRNA
525 degradation, proteolysis of RNase E and increased turnover of ribosome-free

526 transcripts. *Molecular Microbiology* **111**, 1715-1731 (2019).
527 https://doi.org/https://doi.org/10.1111/mmi.14248
528 15 Kim, S., Wang, Y.-H., Hassan, A. & Kim, S. Re-defining how mRNA degradation
529 is coordinated with transcription and translation in bacteria. *bioRxiv* (2024).
530 https://doi.org/10.1101/2024.04.18.588412
531 16 Moffitt, J. R., Pandey, S., Boettiger, A. N., Wang, S. & Zhuang, X. Spatial
532 organization shapes the turnover of a bacterial transcriptome. *eLife* **5**, e13065
533 (2016). https://doi.org/10.7554/eLife.13065
534 17 Murashko, O. N. & Lin-Chao, S. Escherichia coli responds to environmental
535 changes using enolasic degradosomes and stabilized DicF sRNA to alter cellular
536 morphology. *Proceedings of the National Academy of Sciences* **114**, E8025-
537 E8034 (2017). https://doi.org/doi:10.1073/pnas.1703731114
538 18 Gohrbandt, M. *et al.* Low membrane fluidity triggers lipid phase separation and
539 protein segregation in living bacteria. *The EMBO Journal* **41**, e109800 (2022).
540 https://doi.org/https://doi.org/10.15252/embj.2021109800
541 19 Al-Husini, N., Tomares, D. T., Bitar, O., Childers, W. S. & Schrader, J. M. α-
542 Proteobacterial RNA degradosomes assemble liquid-liquid phase-separated
543 RNP bodies. *Molecular Cell* **71**, 1027-1039.e1014 (2018).
544 https://doi.org/https://doi.org/10.1016/j.molcel.2018.08.003
545 20 Lehnik-Habrink, M. *et al.* RNase Y in Bacillus subtilis: a natively disordered
546 protein that is the functional equivalent of RNase E from Escherichia coli. *Journal
547 of Bacteriology* **193**, 5431-5441 (2011). https://doi.org/doi:10.1128/jb.05500-11
548 21 Callaghan, A. J. *et al.* Studies of the RNA degradosome-organizing domain of the
549 Escherichia coli ribonuclease RNase E. *Journal of Molecular Biology* **340**, 965-
550 979 (2004). https://doi.org/https://doi.org/10.1016/j.jmb.2004.05.046
551 22 Lopez, P. J., Marchand, I., Joyce, S. A. & Dreyfus, M. The C-terminal half of
552 RNase E, which organizes the Escherichia coli degradosome, participates in
553 mRNA degradation but not rRNA processing in vivo. *Molecular Microbiology* **33**,
554 188-199 (1999). https://doi.org/https://doi.org/10.1046/j.1365-2958.1999.01465.x
555 23 Leroy, A., Vanzo, N. F., Sousa, S., Dreyfus, M. & Carpousis, A. J. Function in
556 Escherichia coli of the non-catalytic part of RNase E: role in the degradation of
557 ribosome-free mRNA. *Molecular Microbiology* **45**, 1231-1243 (2002).
558 https://doi.org/https://doi.org/10.1046/j.1365-2958.2002.03104.x
559 24 Islam, M. S., Bandyra, K. J., Chao, Y., Vogel, J. & Luisi, B. F. Impact of
560 pseudouridylation, substrate fold, and degradosome organization on the
561 endonuclease activity of RNase E. *RNA* **27**, 1339-1352 (2021).
562 https://doi.org/10.1261/rna.078840.121
563 25 Zhang, M. *et al.* Rational design of true monomeric and bright photoactivatable
564 fluorescent proteins. *Nature Methods* **9**, 727-729 (2012).
565 https://doi.org/10.1038/nmeth.2021
566 26 Jaqaman, K. *et al.* Robust single-particle tracking in live-cell time-lapse
567 sequences. *Nature Methods* **5**, 695-702 (2008).
568 https://doi.org/10.1038/nmeth.1237
569 27 Paintdakhi, A. *et al.* Oufti: an integrated software package for high-accuracy,
570 high-throughput quantitative microscopy analysis. *Molecular Microbiology* **99**,
571 767-777 (2016). https://doi.org/https://doi.org/10.1111/mmi.13264

28 Abramson, J. *et al.* Structure and mechanism of the lactose permease of Escherichia coli. *Science* **301**, 610-615 (2003). https://doi.org/doi:10.1126/science.1088196

29 Ahrem, B., Hoffschulte, H. K. & Müller, M. In vitro membrane assembly of a polytopic, transmembrane protein results in an enzymatically active conformation. *J Cell Biol* **108**, 1637-1646 (1989). https://doi.org/10.1083/jcb.108.5.1637

30 Nagamori, S., Vázquez-Ibar, J. L., Weinglass, A. B. & Kaback, H. R. In vitro synthesis of lactose permease to probe the mechanism of membrane insertion and folding. *Journal of Biological Chemistry* **278**, 14820-14826 (2003). https://doi.org/https://doi.org/10.1074/jbc.M300332200

31 Stochaj, U. & Ehring, R. The N-terminal region of Escherichia coli lactose permease mediates membrane contact of the nascent polypeptide chain. *European Journal of Biochemistry* **163**, 653-658 (1987). https://doi.org/https://doi.org/10.1111/j.1432-1033.1987.tb10914.x

32 Volkov, I. L. *et al.* Spatiotemporal kinetics of the SRP pathway in live E. coli cells. *Proceedings of the National Academy of Sciences* **119**, e2204038119 (2022). https://doi.org/doi:10.1073/pnas.2204038119

33 Thappeta, Y. *et al.* Glycogen phase separation drives macromolecular rearrangement and asymmetric division in E. coli. *bioRxiv* (2024). https://doi.org/10.1101/2024.04.19.590186

34 Savin, T. & Doyle, P. S. Static and dynamic errors in particle tracking microrheology. *Biophysical Journal* **88**, 623-638 (2005). https://doi.org/10.1529/biophysj.104.042457

35 Bakshi, S., Siryaporn, A., Goulian, M. & Weisshaar, J. C. Superresolution imaging of ribosomes and RNA polymerase in live Escherichia coli cells. *Molecular Microbiology* **85**, 21-38 (2012). https://doi.org/https://doi.org/10.1111/j.1365-2958.2012.08081.x

36 Sanamrad, A. *et al.* Single-particle tracking reveals that free ribosomal subunits are not excluded from the Escherichia coli nucleoid. *Proceedings of the National Academy of Sciences* **111**, 11413-11418 (2014). https://doi.org/doi:10.1073/pnas.1411558111

37 Stracy, M. *et al.* Live-cell superresolution microscopy reveals the organization of RNA polymerase in the bacterial nucleoid. *Proceedings of the National Academy of Sciences* **112**, E4390-E4399 (2015). https://doi.org/doi:10.1073/pnas.1507592112

38 Mosteller, R. D. & Yanofsky, C. Transcription of the tryptophan operon in Escherichia coli: Rifampicin as an inhibitor of initiation. *Journal of Molecular Biology* **48**, 525-531 (1970). https://doi.org/https://doi.org/10.1016/0022-2836(70)90064-1

39 Binenbaum, Z., Parola, A. H., Zaritsky, A. & Fishov, I. Transcription- and translation-dependent changes in membrane dynamics in bacteria: testing the transertion model for domain formation. *Molecular Microbiology* **32**, 1173-1182 (1999). https://doi.org/https://doi.org/10.1046/j.1365-2958.1999.01426.x

616 40 Matsumoto, K., Hara, H., Fishov, I., Mileykovskaya, E. & Norris, V. The
617 membrane: transertion as an organizing principle in membrane heterogeneity.
618 *Frontiers in Microbiology* **6**, 572 (2015). https://doi.org/10.3389/fmicb.2015.00572
619 41 Bellotto, N. *et al.* Dependence of diffusion in Escherichia coli cytoplasm on
620 protein size, environmental conditions, and cell growth. *eLife* **11**, e82654 (2022).
621 https://doi.org/10.7554/eLife.82654
622 42 Linnik, D., Maslov, I., Punter, C. M. & Poolman, B. Dynamic structure of E. coli
623 cytoplasm: supramolecular complexes and cell aging impact spatial distribution
624 and mobility of proteins. *Communications Biology* **7**, 508 (2024).
625 https://doi.org/10.1038/s42003-024-06216-3
626 43 Chandran, V. & Luisi, B. F. Recognition of enolase in the Escherichia coli RNA
627 degradosome. *Journal of Molecular Biology* **358**, 8-15 (2006).
628 https://doi.org/https://doi.org/10.1016/j.jmb.2006.02.012
629 44 Chandran, V. *et al.* Recognition and cooperation between the ATP-dependent
630 RNA helicase RhlB and ribonuclease RNase E. *Journal of Molecular Biology*
631 **367**, 113-132 (2007). https://doi.org/https://doi.org/10.1016/j.jmb.2006.12.014
632 45 Nurmohamed, S., McKay, A. R., Robinson, C. V. & Luisi, B. F. Molecular
633 recognition between Escherichia coli enolase and ribonuclease E. *Acta*
634 *Crystallographica Section D* **66**, 1036-1040 (2010).
635 https://doi.org/doi:10.1107/S0907444910030015
636 46 Nurmohamed, S., Vaidialingam, B., Callaghan, A. J. & Luisi, B. F. Crystal
637 structure of Escherichia coli polynucleotide phosphorylase core bound to RNase
638 E, RNA and manganese: implications for catalytic mechanism and RNA
639 degradosome assembly. *Journal of Molecular Biology* **389**, 17-33 (2009).
640 https://doi.org/https://doi.org/10.1016/j.jmb.2009.03.051
641 47 Stark, H. *et al.* The 70S Escherichia coli ribosome at 23 å resolution: fitting the
642 ribosomal RNA. *Structure* **3**, 815-821 (1995).
643 https://doi.org/https://doi.org/10.1016/S0969-2126(01)00216-7
644 48 Dai, X. *et al.* Reduction of translating ribosomes enables Escherichia coli to
645 maintain elongation rates during slow growth. *Nature Microbiology* **2**, 16231
646 (2016). https://doi.org/10.1038/nmicrobiol.2016.231
647 49 Miller, C. C. & Walker, J. The Stokes-Einstein law for diffusion in solution.
648 *Proceedings of the Royal Society of London. Series A, Containing Papers of a*
649 *Mathematical and Physical Character* **106**, 724-749 (1924).
650 https://doi.org/doi:10.1098/rspa.1924.0100
651 50 Saffman, P. G. & Delbrück, M. Brownian motion in biological membranes.
652 *Proceedings of the National Academy of Sciences* **72**, 3111-3113 (1975).
653 https://doi.org/doi:10.1073/pnas.72.8.3111
654 51 Papanastasiou, M. *et al.* The Escherichia coli peripheral inner membrane
655 proteome. *Molecular & Cellular Proteomics* **12**, 599-610 (2013).
656 https://doi.org/10.1074/mcp.M112.024711
657 52 Phillips, J. C. *et al.* Scalable molecular dynamics with NAMD. *Journal of*
658 *Computational Chemistry* **26**, 1781-1802 (2005).
659 https://doi.org/https://doi.org/10.1002/jcc.20289
660 53 Schuck, A., Diwa, A. & Belasco, J. G. RNase E autoregulates its synthesis in
661 Escherichia coli by binding directly to a stem-loop in the rne 5′ untranslated

662 region. *Molecular Microbiology* **72**, 470-478 (2009).
663 https://doi.org/https://doi.org/10.1111/j.1365-2958.2009.06662.x
664 54 Apirion, D. Isolation, genetic mapping and some characterization of a mutation in
665 Escherichia coli that affects the processing of ribonucleic acid. *Genetics* **90**, 659-
666 671 (1978). https://doi.org/10.1093/genetics/90.4.659
667 55 Bessarab, D. A., Kaberdin, V. R., Wei, C.-L., Liou, G.-G. & Lin-Chao, S. RNA
668 components of Escherichia coli degradosome: evidence for rRNA decay.
669 *Proceedings of the National Academy of Sciences* **95**, 3157-3161 (1998).
670 https://doi.org/doi:10.1073/pnas.95.6.3157
671 56 Ghora, B. K. & Apirion, D. Structural analysis and in vitro processing to p5 rRNA
672 of a 9S RNA molecule isolated from an rne mutant of E. coli. *Cell* **15**, 1055-1066
673 (1978). https://doi.org/https://doi.org/10.1016/0092-8674(78)90289-1
674 57 Li, Z., Pandit, S. & Deutscher, M. P. RNase G (CafA protein) and RNase E are
675 both required for the 5′ maturation of 16S ribosomal RNA. *The EMBO Journal* **18**,
676 2878-2885 (1999). https://doi.org/https://doi.org/10.1093/emboj/18.10.2878
677 58 Roy, M. K., Singh, B., Ray, B. K. & Apirion, D. Maturation of 5-S rRNA:
678 ribonuclease E cleavages and their dependence on precursor sequences.
679 *European Journal of Biochemistry* **131**, 119-127 (1983).
680 https://doi.org/https://doi.org/10.1111/j.1432-1033.1983.tb07238.x
681 59 Li, Z. & Deutscher, M. P. RNase E plays an essential role in the maturation of
682 Escherichia coli tRNA precursors. *RNA* **8**, 97-109 (2002).
683 60 Ow, M. C. & Kushner, S. R. Initiation of tRNA maturation by RNase E is essential
684 for cell viability in E. coli. *Genes & Development* **16**, 1102-1115 (2002).
685 https://doi.org/10.1101/gad.983502
686 61 Ikeda, Y., Yagi, M., Morita, T. & Aiba, H. Hfq binding at RhlB-recognition region
687 of RNase E is crucial for the rapid degradation of target mRNAs mediated by
688 sRNAs in Escherichia coli. *Molecular Microbiology* **79**, 419-432 (2011).
689 https://doi.org/https://doi.org/10.1111/j.1365-2958.2010.07454.x
690 62 Reyer, M. A. *et al.* Kinetic modeling reveals additional regulation at co-
691 transcriptional level by post-transcriptional sRNA regulators. *Cell Reports* **36**,
692 109764 (2021). https://doi.org/https://doi.org/10.1016/j.celrep.2021.109764
693 63 Liou, G.-G., Jane, W.-N., Cohen, S. N., Lin, N.-S. & Lin-Chao, S. RNA
694 degradosomes exist in vivo in Escherichia coli as multicomponent complexes
695 associated with the cytoplasmic membrane via the N-terminal region of
696 ribonuclease E. *Proceedings of the National Academy of Sciences* **98**, 63-68
697 (2001). https://doi.org/doi:10.1073/pnas.98.1.63
698 64 Szeto, T. H., Rowland, S. L., Habrukowich, C. L. & King, G. F. The MinD
699 membrane targeting sequence is a transplantable lipid-binding helix. *Journal of*
700 *Biological Chemistry* **278**, 40050-40056 (2003).
701 https://doi.org/https://doi.org/10.1074/jbc.M306876200
702 65 Bayas, C. A. *et al.* Spatial organization and dynamics of RNase E and ribosomes
703 in Caulobacter crescentus. *Proceedings of the National Academy of Sciences*
704 **115**, E3712-E3721 (2018). https://doi.org/doi:10.1073/pnas.1721648115
705 66 Oviedo-Bocanegra, L. M., Hinrichs, R., Rotter, Daniel Andreas O., Dersch, S. &
706 Graumann, P. L. Single molecule/particle tracking analysis program SMTracker
707 2.0 reveals different dynamics of proteins within the RNA degradosome complex

708 in Bacillus subtilis. *Nucleic Acids Research* **49**, e112-e112 (2021).
709 https://doi.org/10.1093/nar/gkab696
710 67 Kapanidis, A. N., Uphoff, S. & Stracy, M. Understanding protein mobility in
711 bacteria by tracking single molecules. *Journal of Molecular Biology* **430**, 4443-
712 4455 (2018). https://doi.org/https://doi.org/10.1016/j.jmb.2018.05.002
713 68 Gray, W. T. *et al.* Nucleoid size scaling and intracellular organization of
714 translation across bacteria. *Cell* **177**, 1632-1648.e1620 (2019).
715 https://doi.org/https://doi.org/10.1016/j.cell.2019.05.017
716 69 Volkov, I. L. *et al.* tRNA tracking for direct measurements of protein synthesis
717 kinetics in live cells. *Nature Chemical Biology* **14**, 618-626 (2018).
718 https://doi.org/10.1038/s41589-018-0063-y
719 70 Park, S. *et al.* Dynamic interactions between the RNA chaperone Hfq, small
720 regulatory RNAs, and mRNAs in live bacterial cells. *eLife* **10**, e64207 (2021).
721 https://doi.org/10.7554/eLife.64207
722 71 Hamouche, L., Poljak, L. & Carpousis, A. J. Polyribosome-dependent clustering
723 of membrane-anchored RNA degradosomes to form sites of mRNA degradation
724 in Escherichia coli. *mBio* **12**, e1932-1921 (2021).
725 https://doi.org/doi:10.1128/mbio.01932-21
726 72 Hamouche, L. *et al.* Dynamic membrane localization of RNase Y in Bacillus
727 subtilis. *mBio* **11**, e3337-3319 (2020). https://doi.org/doi:10.1128/mbio.03337-19
728 73 Knight, J. D., Lerner, M. G., Marcano-Velázquez, J. G., Pastor, R. W. & Falke,
729 Joseph J. Single molecule diffusion of membrane-bound proteins: window into
730 lipid contacts and bilayer dynamics. *Biophysical Journal* **99**, 2879-2887 (2010).
731 https://doi.org/https://doi.org/10.1016/j.bpj.2010.08.046

732